www.MaterialsViews.com

ADVANCED
FUNCTIONAL
MATERIALS
www.afm-journal.de

FULL PAPER

Hierarchical Layered Double Hydroxide Microspheres with Largely Enhanced Performance for Ethanol Electrooxidation

Mingfei Shao, Fanyu Ning, Jingwen Zhao, Min Wei,* David G. Evans, and Xue Duan

Hierarchical MgFe-layered double hydroxide (LDH) microspheres with tunable interior structure are synthesized by a facile and cost-effective surfactant-templated method. Scanning and transmission electron microscopy images reveal that the obtained microspheres display a three-dimensional architecture with hollow, yolk–shell and solid interior structure, respectively, with continuous changes in specific surface area and pore-size distribution. Moreover, the hollow MgFe-LDH microspheres exhibit excellent electrocatalytic oxidation of ethanol in alkaline fuel cell, including high activity, long-term durability and cycling stability, owing to the significantly improved faradaic redox reaction and mass transport. Therefore, this work provides a promising approach for the design and synthesis of structure tunable materials with largely enhanced ethanol electrooxidation behavior, which can be potentially used in noble metal-free alkaline fuel cells.

1. Introduction

Considerable efforts have been devoted to exploit clean and efficient power sources owing to the increasing demands for low-cost and renewable energy, coupled with concerns over environmental pollution.[1] Ethanol is a promising fuel for low-temperature direct fuel cell reactions because of its high energy density, low toxicity, ease of storage and availability from biomass.[2] Noble metal based materials (Pt, Pd, and their alloy) are the most effective catalysts in direct ethanol fuel cells (DEFCs) due to their superior properties in the adsorption and dissociation of small organic molecules,[3] but the high cost, limited availability as well as unsatisfactory cycle life restrict their practical applications. Some explorations have been made to obtain advanced and sophisticated noble metal-based heterostructures for the purpose of improving the performance of DEFCs anode materials, such as ternary Pt/Rh/SnO$_2$ electrocatalyst,[4] graphene-supported Pt,[5] and free-standing Pd-Based nanomembranes.[6] Despite all these progress, how to develop effective noble metal-free anode catalysts for ethanol electrooxidation remains a challenging goal.

Recently, much attention has been paid to nanostructured materials with hierarchical architecture due to their large specific surface area and good structural stability, as well as largely enhanced electrochemical properties in comparison with their low-dimensional counterparts.[7] Layered double hydroxides (LDHs) are a class of 2D anionic clays[8] which have been widely used in the fields of electrochemical sensors,[9] supercapacitors,[10] alkaline secondary batteries[11] and fuel cells,[12] owing to their desirable properties including low cost, high catalytic activity and stability. Recently, LDHs have been reported as promising noble metal-free electrode materials for the electrocatalytic oxidation of methanol in alkaline medium.[12d] However, the aggregation of LDH powdered samples imposes great influence on the electrocatalytic performance. A key challenge for LDHs in the application of anode materials is to fabricate a well-defined hierarchical architecture with high surface area and suitable pore-size distribution, in which all the electroactive species participates in faradaic redox reaction and a fast mass transport and electron transfer are guaranteed.

Herein, hierarchical MgFe-LDH microspheres with tunable interior architecture from solid to hollow structure were obtained *via* a surfactant-templated reaction, and the hollow microspheres show excellent electrocatalytic oxidation of ethanol in alkaline medium. By controlling the concentration of sodium dodecyl sulfonate (SDS), the structure of the products can be tailored from hierarchical flower-like LDH solid spheres to yolk-shell and then to hollow spheres with dif-ferent interior space. The as-obtained hollow MgFe-LDH microspheres exhibit the most promising behavior in alkaline fuel cell, with a maximum ethanol oxidation current of 1.14 mA cm^{-2}, much larger than that of yolk-shell (0.53 mA cm^{-2}) and solid (0.32 mA cm^{-2}) microspheres. In addition, the hollow microspheres show enhanced long-term durability and cycling stability for ethanol electrooxidation. This work provides a facile approach for the fabrication of hierarchical LDH materials by tuning interior architecture, which can serve as highly efficient noble metal-free anode catalysts in DEFCs.

2. Results and Discussion

The morphology and structure of LDH microspheres were studied by scanning electron microscopy (SEM) and

M. F. Shao, F. Y. Ning, J. W. Zhao, Prof. M. Wei,
Prof. D. G. Evans, Prof. X. Duan
State Key Laboratory of Chemical
Resource Engineering
Beijing University of Chemical Technology
Beijing 100029, P. R. China
E-mail: weimin@mail.buct.edu.cn

**ADVANCED
FUNCTIONAL
MATERIALS**

www.afm-journal.de

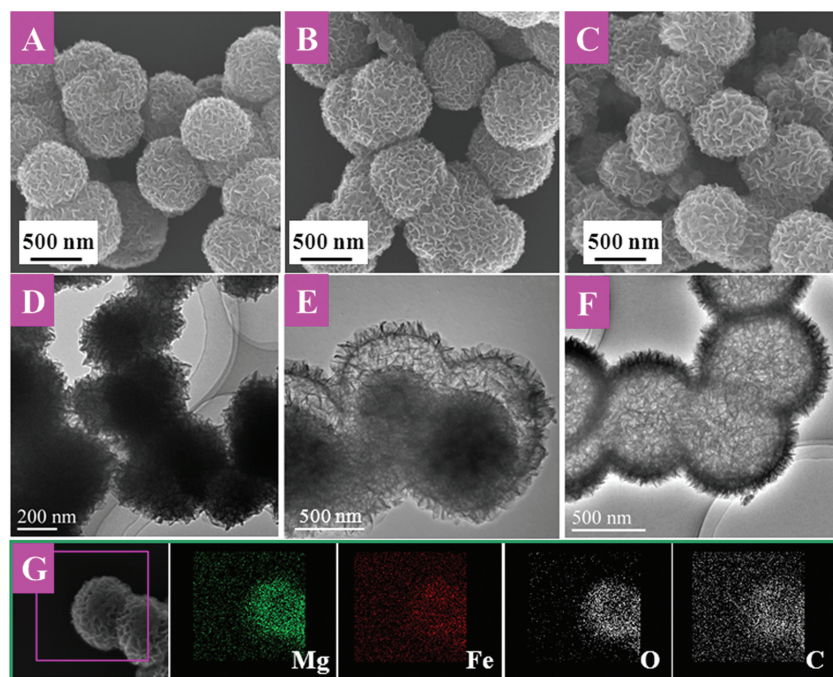FULL PAPER

Materials Views

www.MaterialsViews.com

Figure 1. SEM and TEM images of MgFe-LDH microspheres with different inner architecture: A,D) solid, B,E) yolk-shell, C,F) hollow, and G) EDX mapping results of a single LDH hollow microsphere.

transmission electron microscopy (TEM). **Figure 1**A–C display typical SEM images of MgFe-LDH microspheres obtained with different SDS concentration (see Experimental), illustrating a well-dispersed and spherical morphology with particle size of ~580 nm. The as-synthesized flower-like microspheres are composed of numerous LDH nanoflakes (~80 nm in width and ~20 nm in thickness) as building blocks. The corresponding TEM images (Figure 1D,E,F) reveal solid, yolk-shell and hollow spherical structure, respectively. It can be seen that the shell thickness of hollow LDH microspheres is ~85 nm, close to the lateral size of LDH nanoflakes. The high resolution TEM (HR-TEM) image shows lattice fringes corresponding to an interplanar distance of ~0.24 nm, which can be attributed to the (012) plane of a MgFe-LDH phase (Supporting Information Figure S1). EDX mapping analysis for the hollow LDH microspheres is shown in Figure 1G, from which it is observed that both iron and magnesium are homogeneously distributed throughout the outer shell of microsphere. The EDX spectrum of the microspheres (Supporting Information Figure S2) also shows the presence of Mg and Fe, which is consistent with the mapping results. In addition, the elemental analysis demonstrates that the three samples show rather close Mg/Fe ratio (2.32–2.49, Supporting Information Table S1), indicating that the SDS template does not impose significant influence on the Mg/Fe ratio of LDH microspheres. In order to demonstrate the generality of this approach, NiFe-LDH microspheres were also synthesized *via* the surfactant-templated method by changing the concentration of SDS, giving a similar uniform flower-like morphology with tunable interior architecture from solid to hollow structure (Supporting Information Figure S3).

The powder XRD pattern for MgFe-LDH hollow microspheres (Supporting Information Figure S4) indicates that the product is single-crystalline MgFe-LDH phase (JCPDF card no. 14-0281). However, several weak reflections at $2\theta = 17°, 23°, 42°,$ and $44°$ were observed for the solid and yolk-shell LDH microspheres, which can be assigned to small amount of α-FeOOH impurity (JCPDF card no. 29-713). The FT-IR technique was also used to identify the nature and symmetry of interlayer anions (Supporting Information Figure S5). The spectra of the three samples are rather similar: a broad intense band between 3600 and 3100 cm^{-1} is due to the OH stretching mode of hydroxyl groups in host layers and interlayer water molecules; the band at 1503 cm^{-1} together with its accompanying band at 1380 cm^{-1} is attributed to mode v_3 of interlayer carbonate species.[13] The results confirm the formation of carbonate-containing LDHs for all the three samples. In addition, the characteristic bands of $-SO_3^-$ group at 1251 and 1083 cm^{-1}, combined with the two absorption bands at 2850 and 2920 cm^{-1} corresponding to the antisymmetric and symmetric stretching of $-CH_2$ in the alkyl chain, demonstrate the presence of SDS in the obtained MgFe-LDH microspheres. Elemental analysis results reveal the SDS residue in the LDH materials: solid (3.1 wt%), yolk-shell (4.6 wt%), hollow (6.8 wt%), which is approximately consistent with the results of thermogravimetric analysis (TGA) for the three samples (Supporting Information Figure S6).

Time-dependent experiments were carried out to understand the formation process of such interesting hierarchical hollow LDH microspheres. The XRD patterns of the samples with various reaction time are shown in Supporting Information Figure S7. The LDH sample (4 h: Supporting Information Figure S7a) displays several broad reflections which can be attributed to amorphous pseudoboehmite hydroxide. As the reaction time was extended to 8 h, several weak reflections corresponding to LDH phase appear (Supporting Information Figure S7b), whose intensity increases gradually upon prolonging the hydrothermal treatment time from 8 h to 24 h (Supporting Information Figure S7c), indicating an enhancement in the crystallinity of LDH phase. **Figure 2** shows the SEM and TEM images of the three samples obtained with different reaction duration. The SEM image of LDH material (4 h) shows the agglomerates of nanoparticles (~27 nm) (Figure 2A). Numerous nanoflakes come into formation on the surface of microspheres with the reaction time of 8 h (Figure 2B). As the reaction time was further increased to 24 h, intercrossing nanoflakes with well-defined plate-like morphology appear in the SEM image (Figure 2C). The SEM results coincide with those of the XRD patterns, indicating the crystallinity of LDH phase increases along with reaction time. Moreover, it can be seen that the shell thickness can be tuned by varying the reaction time (Figure 2D–F). The outer shell thickness of LDH hollow microspheres increases from ~58 to ~120 nm upon prolonging the reaction time from 4 to

Materials
Views
www.MaterialsViews.com

ADVANCED
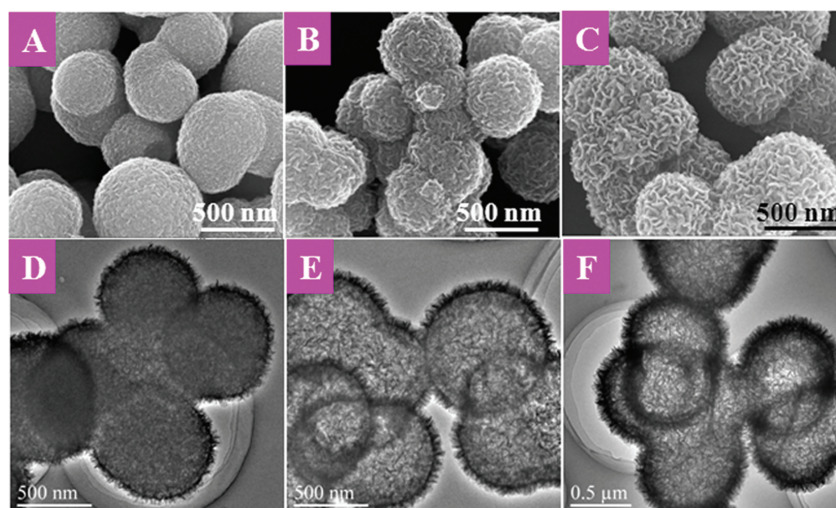FUNCTIONAL
MATERIALS
www.afm-journal.de

Figure 2. SEM and TEM images of MgFe-LDH microspheres synthesized with different reaction time: A,D) 4 h, B,E) 8 h, and C,F) 24 h.

24 h, while the inner diameter of LDH microspheres remains unchanged.

According to the above experimental observations, the formation process of LDH microspheres by surfactant-templated method can be roughly divided into two stages (**Figure 3**): the first step involves the adsorption of di- and tri-valence metal ions on the hydrophilic end of SDS by electrostatic interaction and the formation of SDS-metal ions spheroidal reverse micelles; the second step consists of the nucleation and growth of LDH phase in the inner space of SDS micelle, forming the resulting hierarchical LDH microspheres. The concentration of SDS is responsible for the formation of microspheres with tunable inner architecture. A lower concentration induces less SDS micelle in the reaction system and a high density of LDH nanoparticles precursor wrapped in the core of per micelle; this
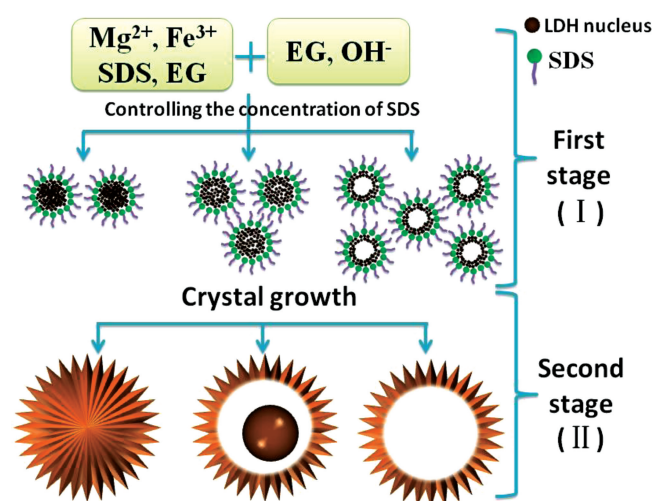
would lead to the achievement of solid LDH microspheres. In contrast, a higher concentration of SDS results in the formation of yolk-shell and hollow microspheres. Similar explaination has been reported previously for the preparation of metal alloy and metal oxide spheres.[14] TGA measurements of the LDH precursor-SDS micelle (the products of the first stage in Figure 3) further confirm the formation process (Supporting Information Figure S8). It was found that with the increase of SDS concentration from 6.7 g/L to 26.7 g/L, the SDS weight percentage of the precursor micelle increases gradually from 9.1% to 14.9%; while the content of LDH precursor remains almost unchanged. The results indicate that a high SDS concentration leads to a low density of LDH precursor wrapped in the core of micelle, which thereby results in the formation of hollow LDH microspheres (the second stage in Figure 3).

The surface area and pore-size distribution are two key factors for the electroactive materials in electrocatalysis applications. Therefore, the obtained MgFe-LDH samples were investigated for their surface area and porosity property by N_2-adsorption/desorption measurements (**Figure 4**). In all the cases, typical IV isotherms with H3-type hysteresis loops ($P/P_0 > 0.4$) are observed, indicating the presence of mesopores.[15] This type of hysteresis loops does not exhibit any limiting adsorption at high P/P_0 region, which is commonly attributed to particle aggregates with slitshaped pores.[16] Specifically, the maximum specific surface area is presented in the sample of hollow LDH microspheres (213.6 m^2/g), much larger than that of yolk-shell (124.4 m^2/g) and solid (78.8 m^2/g). In addition, the pore size analysis based on the isotherms shows that these samples consist of a mesopore distribution in the range 2–6 nm.

Figure 5 displays the XPS results of Mg 1s, Fe 2p, C 1s and O 1s of MgFe-LDH hollow microspheres. The peaks were decomposed using mixed Gaussian-Lorentzian functions,
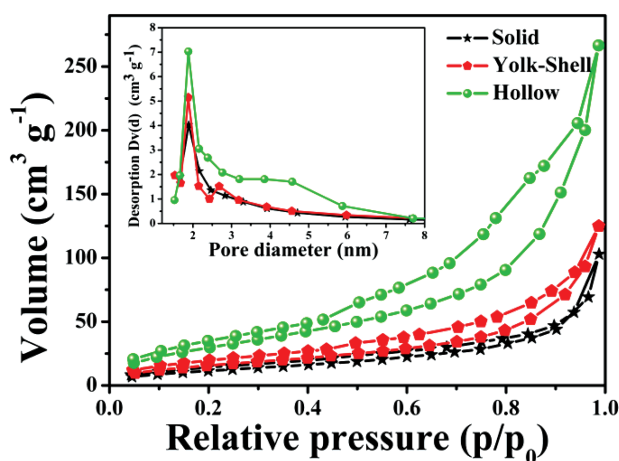

Figure 3. Schematic illustration of the morphological evolution process of the as-obtained flower-like hierarchical LDH microspheres: (I) formation of LDH precursor-SDS micelle; (II) formation of flower-like microspheres with different inner architecture.

Figure 4. N_2-sorption isotherms and pore size distribution (inset) of MgFe-LDH microspheres with different inner architecture: solid (black), yolk-shell (red), hollow (green).
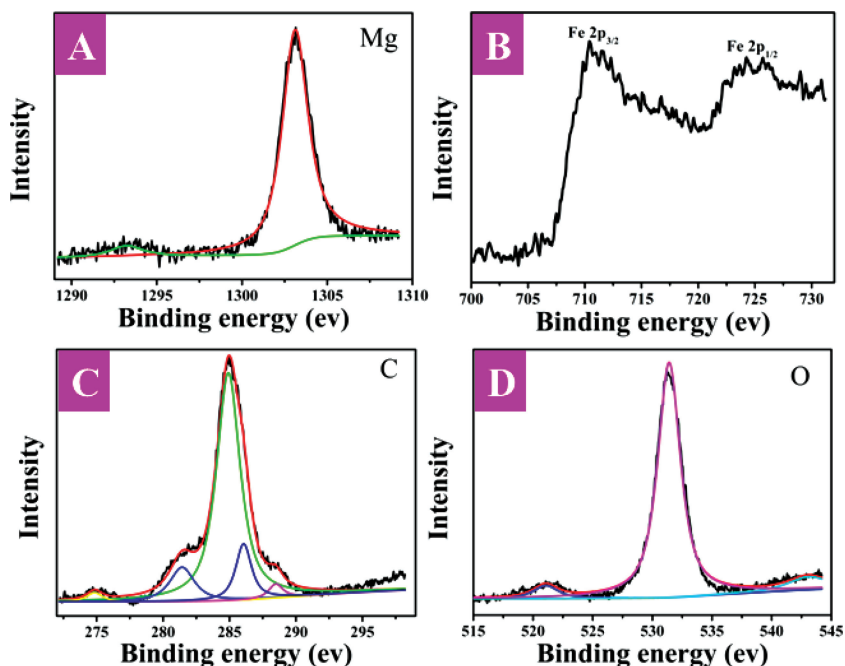
ADVANCED
FUNCTIONAL
MATERIALS
www.afm-journal.de

Materials Views
www.MaterialsViews.com

FULL PAPER

Figure 5. A) Mg 1s, B) Fe 2p, C) C 1s, and D) O 1s orbital XPS spectra for the LDH hollow microspheres.

nonlinear squares fitting algorithm, and Shirley-type background subtraction by using XPS peak fit software. The binding energy of Mg 1s is 1303.2 eV, indicating the Mg (II) oxidation state in the sample (Figure 5A). As shown in Figure 5B, the Fe 2p doublet (Fe $2p_{3/2}$ and $2p_{1/2}$) is located at 710.5 and 724.5 eV, corresponding to the trivalent state of Fe (III). The presence of C 1s peak (285.5 eV) was mainly contributed by the interlayer carbonate group of LDH material (Figure 5C). The deconvolution of the O 1s peak results in three peaks with the Gaussian shape, corresponding to O^{2-}, OH^- and H_2O, respectively.[17]

The catalytic activity of MgFe-LDH microspheres with different inner architecture towards ethanol electrooxidation was subsequently evaluated in an alkaline medium. The oxidation current was normalized to the electroactive surface area; this allowed the current density to be directly used to compare the catalytic activity of different samples. The cyclic voltammograms (CVs) of the three catalysts recorded in 1.0 M NaOH solution without ethanol are shown in Supporting Information Figure S9. Each CV curve of the LDH microspheres consists of a pair of redox peaks, corresponding to the reversible redox of Fe^{2+}/Fe^{3+} associated with OH^-. However, the redox current is significantly enhanced for the MgFe-LDH hollow microspheres modified electrode in comparison with the yolk-shell, solid microspheres and MgFe-LDH nanoparticles, highlighting the importance of the LDH nanostructure to its electroactivity performance. In the presence of 1.0 M ethanol, the MgFe-LDH nanoparticles almost show no electrocatalytic property to the oxidation of ethanol (**Figure 6**A, blue line). In the contrast, all the three types of MgFe-LDH microspheres display electrocatalytic behavior. The MgFe-LDH hollow microspheres catalyst exhibits the highest electrocatalytic activity with a reverse

oxidation current density of 1.14 mA cm^{-2} at ~0.45 V, much larger than that of the yolk-shell (0.53 mA cm^{-2}) and solid one (0.32 mA cm^{-2}) (Figure 6A). In addition, its electrooxidation current shows a linear increase with the increase of ethanol concentration from 0.5 to 2.0 M, further demonstrating the remarkable catalytic activity (Supporting Information Figure S10). The enhancement in the electrooxidation performance of the hollow LDH microspheres is mainly attributed to the specific nanostructure with large surface area, which provides more electroactive sites as well as effective diffusion channels for the electrolyte ions (OH^-). In particular, the abundant mesopores in the structure benefit the mass diffusion and electron transfer, which guarantees highly efficient electrooxidation reaction. The enhanced electrochemical behavior of the hollow microspheres was further verified by the electrochemical impedance spectroscopy (EIS) measurements. Supporting Information Figure S11 shows the Nyquist plots of the EIS spectra for hollow, yolk-shell, solid and LDH nanoparticles, respectively. The semicircle-like shape for the EIS spectra of these samples was observed with the following sequence of the electron transfer resistance (R_{et}):[18] hollow< yolk-shell < solid < LDH nanoparticles, which clearly demonstrates that the hollow structure possesses lower resistance and thus allows for much faster electron transfer. The electrical conductivity measurements further show that the hollow LDH microspheres sample possesses larger electrical conductivity than the solid and yolk-shell sample (Supporting Information Figure S12), which is consistent with the results of EIS.

To evaluate the electrocatalytic activity and stability of MgFe-LDH microspheres under continuous operating conditions, long-term chronoamperometric tests were carried out in a 1.0 M NaOH + 1.0 M ethanol solution. Figure 6B shows the current density curves versus time recorded at 0.45 V for 3600 s. It was found that the oxidation current density of the hollow microspheres is much higher than that of the yolk-shell, solid microspheres and LDH nanoparticles, further demonstrating a significantly enhanced electrocatalytic activity. Moreover, the time consumption is ~20 min for 50% current decay in the case of hollow microspheres; whereas ~6 min and ~3 min are consumed for the yolk–shell and solid microspheres, respectively. This indicates that the LDH hollow microspheres catalyst exhibits largely enhanced long-term durability for ethanol electrooxidation in alkaline media. In addition, the cycling stability of the three MgFe-LDH microspheres samples was also studied by testing CV cycling, as shown in Figure 6C,D. After 100 potential cycles, 88.7% of the initial catalytic activity was still maintained for the hollow microspheres (Figure 6C) without obvious change in its morphology (Figure S13). This is highly superior to the yolk-shell (65.7%) and solid sample (51.6%) (Figure 6D), indicating the greatly improved stability of the hollow microspheres.
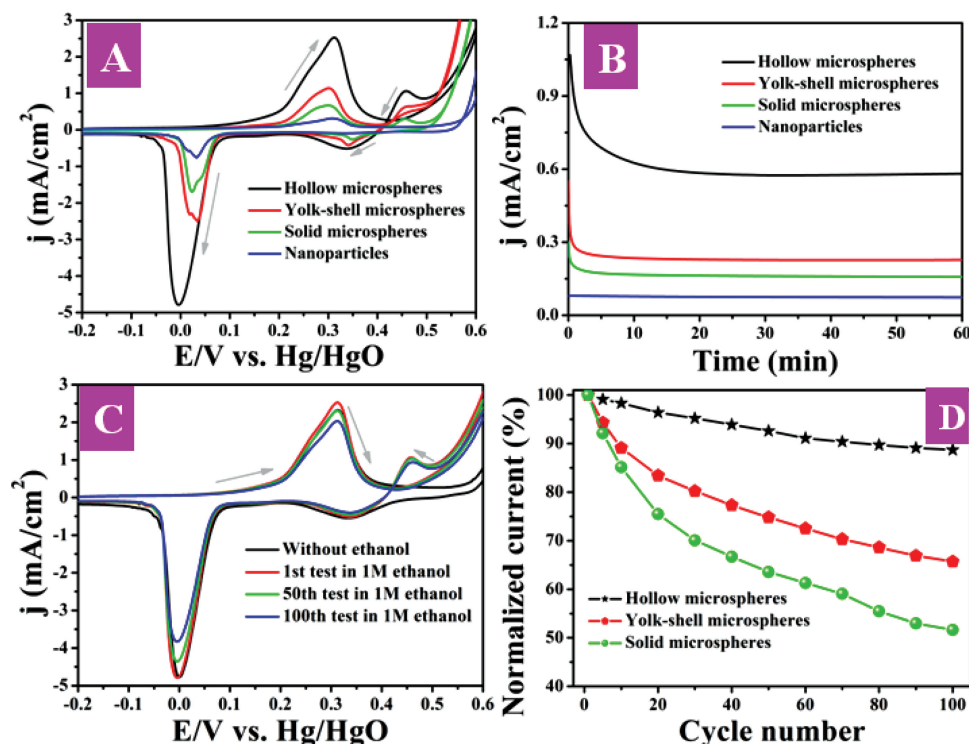
Figure 6. A) Cyclic voltammograms and B) chronoamperometric curves at 0.45 V for ethanol electrooxidation at the MgFe-LDH microspheres modified electrodes: hollow (black), yolk-shell (red), hollow (green), nanoparticles (blue); C) CVs (1st, 50th, and 100th cycle) of the LDH hollow microspheres for ethanol electrooxidation at 50 mV s^{-1}; D) potential cycling stability of MgFe-LDH microspheres with different inner architecture.

3. Conclusions

In conclusion, hierarchical LDH microspheres with tunable interior architecture were synthesized by a facile and cost-effective surfactant-templated approach for highly efficient ethanol electrooxidation. By controlling the concentration of SDS, the obtained microspheres exhibit a three-dimensional architecture with hollow, yolk-shell and solid interior structure, respectively. The hollow LDH microspheres display excellent catalytic activity and robust durability for ethanol electrooxidation, compared with the yolk-shell and solid structure. This can be ascribed to the specific 3D architecture with enhanced surface area and suitable mesopore distribution, which benefits the mass transport of electrolytes and improves the faradaic redox reaction. It is expected that the approach for tuning the interior structure of LDH microspheres can be extended to other oxide or hydroxide materials for potential applications in fuel cells and catalysis.

4. Experimental Section

Synthesis of Hierarchical LDH Microspheres: In a typical synthesis, FeCl$_3$·6H$_2$O (0.180 g) and Mg(NO$_3$)$_2$·6H$_2$O (0.396 g) were dissolved in 20 mL of ethylene glycol under stirring, followed by addition of 0.2, 0.6, 0.8 g of SDS respectively with continuous stirring until complete dissolution. Separately, 0.16 g of NaOH was dissolved in 10 mL of ethylene glycol in another flask. The NaOH solution was added to the mixed solution with vigorous stirring. The mixture was then transferred

into an autoclave, sealed, and heated at 160 °C for 24 h. The precipitate was collected and washed with deionized water and ethanol thoroughly, and then dried at 60 °C for 12 h.

Material Characterization: Powder X-ray diffraction patterns of the microsphere samples were collected on a Shimadzu XRD-6000 diffractometer using a Cu Kα source, with a scan step of 0.02° and a scan range between 3° and 80°. The morphology of the microspheres was investigated using a scanning electron microscope (SEM; Zeiss SUPRA 55) with an accelerating voltage of 20 kV, combined with energy dispersive X-ray spectroscopy (EDX). Transmission electron microscopy (TEM) images were recorded with Philips Tecnai 20 and JEOL JEM-2010 HR-TEM. The accelerating voltage was 200 kV in each case. The specific surface area, pore volume and size analysis were performed by Brunauer–Emmett–Teller (BET) and Barrett–Joyner–Halenda (BJH) methods, respectively, using a Quantachrome Autosorb-1C-VP Analyzer. Prior to the measurements, the samples were degassed at 100 °C for 6 h.

Electrochemical Characterization: Electrochemical measurements were performed on an electrochemical workstation (CHI 660C, CH Instruments Inc., Shanghai) using a three-electrode mode. Pt wire was used as a counter electrode, Hg/HgO as a reference electrode, and glassy carbon (3 mm in diameter) coated with LDH microspheres, as a working electrode. The working electrode was fabricated as follows: 1 mg of LDH microspheres was dispersed in 1 mL of ethanol solution and sonicated for 2 min; 20 μL of the suspension was dripped onto the surface of a glassy carbon electrode and dried for 15 min; subsequently 10 μL of 5% Nafion solution (Sigma–Aldrich) was coated on the surface and dried for another 10 min. Electrocatalytic oxidation of ethanol on the working electrode was measured in 1.0 M KOH electrolyte by cyclic voltammetry in the potential range from −0.2 to +0.6 V. Electrical current density was calculated by normalizing electrical current of glassy carbon electrode with diameter of 3 mm.

FULL PAPER

Supporting Information

Supporting Information is available from the Wiley Online Library or from the author.

[1] a) E. P. Murray, T. Tsai, S. A. Barnett, *Nature* **1999**, *400*, 649; b) J. R. Miller, P. Simon, *Science* **2008**, *321*, 651; c) P. Simon, Y. Gogotsi, *Nat. Mater.* **2008**, *7*, 845; d) C. Xu, H. Wang, P. K. Shen, S. P. Jiang, *Adv. Mater.* **2007**, *19*, 4256; e) S. A. Freunberger, Y. Chen, Z. Peng, J. M. Griffin, L. J. Hardwick, F. Barde, P. Novak, P. G. Bruce, *J. Am. Chem. Soc.* **2011**, *133*, 8040; f) B. Dunn, H. Kamath, J. M. Tarascon, *Science* **2011**, *334*, 928.

[2] a) C. Lamy, E. M. Belgsir, J. M. Leger, *J. Appl. Electrochem.* **2001**, *31*, 799; b) F. Joensen, J. R. Rostrup-Nielsen, *J. Power Sources* **2002**, *105*, 195; c) E. Casado-Rivera, D. J. Volpe, L. Alden, C. Lind, C. Downie, T. Vazquez-Alvarez, A. C. D. Angelo, F. J. DiSalvo, H. D. Abruna, *J. Am. Chem. Soc.* **2004**, *126*, 4043; d) E. Antolini, *J. Power Sources* **2007**, *170*, 1.

[3] a) A. S. Arico, S. Srinavasan, V. Antonucci, *Fuel Cells* **2001**, *1*, 133; b) N. Mackiewicz, G. Surendran, H. Remita, B. Keita, G. Zhang, L. Nadjo, A. Hagege, E. Doris, C. Mioskowski, *J. Am. Chem. Soc.* **2008**, *130*, 8110; c) W. Du, K. E. Mackenzie, D. F. Milano, N. A. Deskins, D. Su, X. Teng, *ACS Catal.* **2012**, *2*, 287.

[4] A. Kowal, M. Li, M. Shao, K. Sasaki, M. B. Vukmirovic, J. Zhang, N. S. Marinkovic, P. Liu, A. I. Frenkel, R. R. Adzic, *Nat. Mater.* **2009**, *8*, 325.

[5] a) L. Dong, R. R. S. Gari, Z. Li, M. M. Craig, S. Hou, *Carbon* **2010**, *48*, 781; b) H. Zhang, X. Xu, P. Gu, C. Li, P. Wu, C. Cai, *Electrochim. Acta* **2011**, *56*, 7064.

[6] H. Wu, H. Li, Y. Zhai, X. Xu, Y. Jin, *Adv. Mater.* **2012**, *24*, 1594.

[7] a) Y. G. Guo, J. S. Hu, L. J. Wan, *Adv. Mater.* **2008**, *20*, 2878; b) S. J. Bao, C. M. Li, J. F. Zang, X. Q. Cui, Y. Qiao, J. Guo, *Adv. Funct. Mater.* **2008**, *18*, 591; c) F. Ksar, L. Ramos, B. Keita, L. Nadjo, P. Beaunier,

H. Remita, *Chem. Mater.* **2009**, *21*, 3677; d) G. G. Wallace, J. Chen, D. Li, S. E. Moulton, J. M. Razal, *J. Mater. Chem.* **2010**, *20*, 3553; e) D. Wang, D. Choi, J. Li, Z. Yang, Z. Nie, R. Kou, D. Hu, C. Wang, L. V. Saraf, J. Zhang, I. A. Aksay, J. Liu, *ACS Nano* **2009**, *3*, 907.

[8] a) Q. Wang, D. O'Hare, *Chem. Rev.* **2012**, *112*, 4124; b) A. M. Fogg, V. M. Green, H. G. Harvey, D. O'Hare, *Adv. Mater.* **1999**, *11*, 1466; c) Z. P. Xu, P. S. Braterman, *J. Phys. Chem. C* **2007**, *111*, 4021; d) J.-H. Choy, S.-Y. Kwak, J.-S. Park, Y.-J. Jeong, J. Portier, *J. Am. Chem. Soc.* **1999**, *121*, 1399; e) Z. Gu, A. C. Thomas, Z. P. Xu, J. H. Campbell, G. Q. Lu, *Chem. Mater.* **2008**, *20*, 3715.

[9] a) D. Shan, S. Cosnier, C. Mousty, *Anal. Chem.* **2003**, *75*, 3872; b) C. Mousty, L. Vieille, S. Cosnier, *Biosens. Bioelectron.* **2007**, *22*, 1733.

[10] a) Z. Gao, J. Wang, Z. Li, W. Yang, B. Wang, M. Hou, Y. He, Q. Liu, T. Mann, P. Yang, M. Zhang, L. Liu, *Chem. Mater.* **2011**, *23*, 3509; b) M. F. Shao, F. Y. Ning, Y. F. Zhao, J. W. Zhao, M. Wei, D. G. Evans, X. Duan, *Chem. Mater.* **2012**, *24*, 1192; c) M. A. Woo, M. S. Song, T. W. Kim, I. Y. Kim, J. Y. Ju, Y. S. Lee, S. J. Kim, J. H. Choy, S. J. Hwang, *J. Mater. Chem.* **2011**, *21*, 4286.

[11] a) P. V. Kamath, G. H. A. Therese, *J. Solid State Chem.* **1997**, *128*, 38; b) A. Sugimoto, S. Ishida, K. Hanawa, *J. Electrochem. Soc.* **1999**, *146*, 1251; c) H. Chen, J. M. Wang, T. Pan, Y. L. Zhao, J. Q. Zhang, C. N. Cao, *J. Electrochem. Soc.* **2003**, *150*, 1399.

[12] a) K. Tadanaga, Y. Furukawa, A. Hayashi, M. Tatsumisago, *J. Electrochem. Soc.* **2012**, *159*, 368; b) S. N. Ding, M. Holzinger, C. Mousty, S. Cosnier, *J. Power Sources* **2010**, *195*, 4714; c) Y. Wang, H. Ji, W. Peng, L. Liu, F. Gao, M. Li, *Int. J. Hydrogen Energy* **2012**, *37*, 9324; d) Y. Wang, D. Zhang, W. Peng, L. Liu, M. Li, *Electrochim. Acta* **2011**, *56*, 5754.

[13] a) J. T. Kloprogge, D. Wharton, L. Hickey, R. L. Frost, *Am. Mineral.* **2002**, *87*, 623; b) G. A. Caravaggio, C. Detellier, Z. Wronski, *J. Mater. Chem.* **2001**, *11*, 912.

[14] a) G. Chen, D. Xia, Z. Nie, Z. Wang, L. Wang, L. Zhang, J. Zhang, *Chem. Mater.* **2007**, *19*, 1840; b) X. J. Wu, D. S. Xu, *J. Am. Chem. Soc.* **2009**, *131*, 2774; c) B. Wang, H. Wu, L. Yu, R. Xu, T. T. Lim, X. W. Lou, *Adv. Mater.* **2012**, *24*, 1111.

[15] J. Yu, J. C. Yu, M. K.-P. Leung, W. Ho, B. Cheng, X. J. Zhao, J. C. Zhao, *J. Catal.* **2003**, *217*, 69.

[16] K. S. W. Sing, D. H. Everett, R. A. W. Haul, L. Moscou, R. A. Pierotti, J. Rouquerol, T. Siemieniewska, *Pure Appl. Chem.* **1985**, *57*, 603.

[17] J. Zhou, Z. P. Xu, S. Qiao, Q. Liu, Y. Xu, G. Qian, *J. Hazard. Mater.* **2011**, *189*, 586.

[18] a) J. F. Zang, S. J. Bao, C. M. Li, H. J. Bian, X. Q. Cui, Q. L. Bao, C. Q. Sun, J. Guo, K. R. Lian, *J. Phys. Chem. C* **2008**, *112*, 14843; b) A. D. Fabio, A. Giorgi, M. Mastragostino, F. Soavi, *J. Electrochem. Soc.* **2001**, *148*, A845.